Progress in InGaAs–GaAs Selective-Area MOCVD Toward Photonic Integrated Circuits

J. J. Coleman, *Fellow, IEEE,* R. M. Lammert, *Student Member, IEEE*, M. L. Osowski, *Student Member, IEEE*, and A. M. Jones, *Student Member, IEEE*

(Invited Paper)

***Abstract*—The progress toward integrated photonic devices by selective-area metalorganic chemical vapor deposition (MOCVD) is reviewed. Processing steps involved with fabricating buried heterostructures (BH's) by a three-step technique are outlined, and a computational model is presented that predicts the enhancement behavior of selective-area MOCVD. Results are reviewed for several discrete and integrated photonic devices. These include low-threshold BH lasers, laser diodes integrated with either intracavity or external cavity modulators, dual-channel emitters integrated with both modulators and passive y-junction waveguides, and broad-band light-emitting diodes (LED's).**

***Index Terms*— Crystal growth, integrated optoelectronics, quantum-well lasers, semiconductor growth, semiconductor lasers, semiconductor materials, strain.**

I. Introduction

BURIED heterostructure (BH) lasers have been fabricated by a variety of techniques [1]–[9]. The most common method involves growing the entire laser structure, forming an active region mesa by wet or dry etching, and regrowing the burying layer [2]. For InGaAs–GaAs–AlGaAs quantum-well (QW) lasers, this method exposes the easily oxidized AlGaAs optical confining layer and requires the subsequent regrowth of AlGaAs on AlGaAs. Since oxides of AlGaAs have desorption temperatures much higher than normal growth temperatures, they remain on the device causing poor crystalline quality and an optically lossy interface region. Etched-mesa BH lasers have been fabricated by hybrid growth techniques using either metalorganic chemical vapor deposition (MOCVD) or molecular beam epitaxy (MBE) for the initial growth and liquid phase epitaxy (LPE) for the regrowth [3]–[7]. All-MOCVD grown etched-mesa strained-layer BH lasers have been reported that require the use of low aluminum composition cladding layers [1]. It is desirable to fabricate BH lasers without exposing AlGaAs and without initiating regrowth with AlGaAs. This can be accomplished using a three-step selective-area MOCVD process [10]–[12].

Manuscript received April 4, 1997; revised June 30, 1997. This work was supported by the National Science Foundation under Grant ECD89-43166 and Grant DMR89-20 538, by the ARPA Center for Optoelectronic Science and Technology under Grant MDA972-94-1-004, and by the Joint Services Electronics Program under Contract N0014-90-J-1270.

The authors are with the Microelectronics Laboratory, University of Illinois at Urbana-Champaign, Urbana, IL 61801 USA.

Publisher Item Identifier S 1077-260X(97)07498-4.

This selective-area epitaxy (SAE) technique gives the advantage of GaAs on GaAs regrowth for fabricating strained-layer InGaAs–GaAs–AlGaAs BH QW lasers, and additionally provides in-plane bandgap energy control to fabricate BH devices [13] with different emission wavelengths on the same wafer for photonic integrated circuit (PIC) applications. This material variation can be accomplished in a single epitaxial step using a growth-inhibiting mask [14], [15]. Selectively-grown active regions have been utilized to integrate laser diodes with other devices such as waveguides [11], modulators [16]–[18], and detectors [19]. Broad-spectrum light-emitting diodes (LED's) [20], [21], laser arrays for wavelength-division multiplexing (WDM) [22], [23], and ring lasers with y-coupled waveguides [24] have also utilized this in-plane bandgap tailoring feature. SAE also enables the use of high-composition AlGaAs for the burying layer, since no AlGaAs on AlGaAs regrowth is necessary. Additionally, control of the mesa width can be provided by the spacing between pairs of oxide stripes. This gives improved width reproducibility over both wet etched BH lasers where undercutting determines the width and LPE regrown BH lasers where meltback affects the width.

In this paper, we describe the fabrication process, modeling technique, and experimental results for photonic devices utilizing InGaAs–GaAs–AlGaAs BH's fabricated using three-step selective-area MOCVD. Monolithic BH lasers show a wide range of emission wavelengths, which is essential for photonic integration applications, from in-plane bandgap energy control provided by selective-area growth rate enhancement of the strained-layer InGaAs-GaAs active region.

II. Buried Heterostructure Fabrication Process

The devices, fabricated in these studies, were grown by atmospheric pressure MOCVD in a vertical reactor on (100) GaAs:n substrates. The three-step growth process (see Fig. 1), which avoids the difficulties associated with the growth of AlGaAs over oxide, begins with the growth of a GaAs buffer layer, a lower AlGaAs cladding layer, and a thin layer of GaAs to prevent oxidation of the AlGaAs when the sample is removed from the reaction chamber. Next, silicon dioxide (SiO_2) is deposited on the wafer, and the dual stripe mask pattern is transferred using standard photolithographic techniques. After patterning, the sample is returned to the reactor for growth of the InGaAs–GaAs active region ($T_G =$ 625 °C). Following this step, the wafer is again removed from

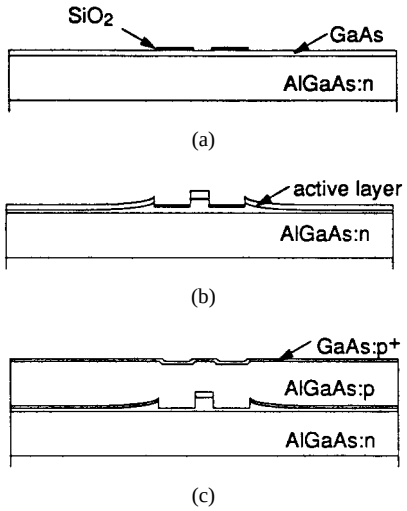

Fig. 1. Growth sequence used in the fabrication of three-step SAE photonic integrated circuits.

the reactor, and the oxide is etched away in a buffered HF solution. Finally, the sample is returned to the reactor for growth of the upper AlGaAs cladding layer and GaAs:p^+ contact layer.

After the growth of the structure is completed, the wafer is patterned with stripes centered directly over the selectively grown active region, and the GaAs:p^+ cap is etched away on either side of the buried ridge to provide additional lateral confinement of the injected carriers. Next, SiO_2 is deposited on the wafer, and contact windows are opened in the oxide. The substrate is lapped and polished to a thickness of $\approx$125 μm, and then n- and p-side metals are deposited. Finally, the sample is cleaved into bars, perpendicular to the stripes, to complete the processing. Shown in Fig. 2 are: (a) an SEM and (b) a schematic cross section of a finished BH laser device.

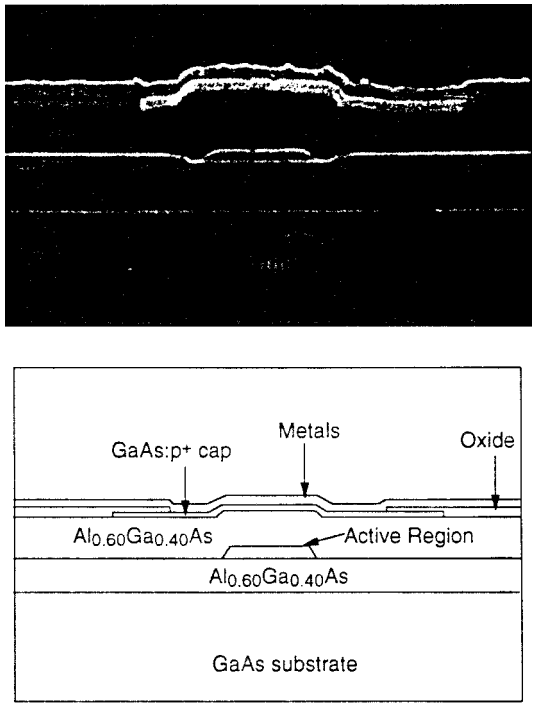

Fig. 2. SEM photograph and corresponding schematic diagram of the cross section of a three-step SAE BH laser.

III. Selective-Area MOCVD Model

In this section, we present the details and simulation results of a computational model for selective-area MOCVD. Diffusion equations and boundary conditions for selective-area MOCVD are applied to predict column III metalorganic source concentrations. Solutions for reaction parameters are found using the finite element method and experimental data. Thickness profiles of InP, GaAs, GaN, InGaAs, and InGaP are accurately calculated with this model providing support for both the validity of the model and the dominance of gas phase diffusion on enhancement.

During selective-area MOCVD, a nonuniform deposition of material occurs across the growth area due to a lithographically-defined growth-inhibiting dielectric mask. Within a stagnant volume of gas (the boundary layer) [25], [26], lateral variations in column III reactant concentrations are induced by the growth mask and are responsible for a nonlinear enhancement of the growth rate across the substrate surface. The SAE model focuses on this boundary layer, and a schematic diagram of the simulation cell with pertinent boundary conditions is shown in Fig. 3. The x and y directions are labeled in the figure, δ is the boundary layer thickness,

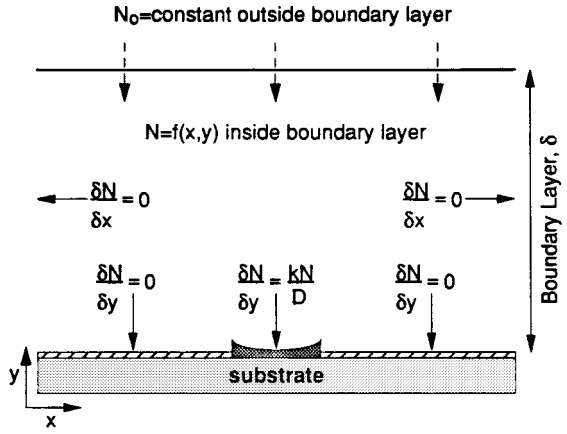

Fig. 3. Schematic diagram of simulation cell used for modeling selective-area MOCVD. Noted in the figure are the boundary conditions applied in the model. Also noted are the x- and y-axes labeled in the lower left corner.

N is the column III source concentration, D is the diffusion coefficient, and k is the reaction rate constant. The empirical parameters N, D, and k are all specific to each column III metalorganic source.

For SAE at atmospheric pressure, gas phase diffusion is widely accepted as the dominant method of enhancement, rather than surface migration, when using growth mask dimensions greater than the surface diffusion length [14], [15], [26]–[29]. Therefore, this SAE model considers only gas phase diffusion of the column III reactants. The boundary layer simulation cell is in general a three-dimensional system, but the model outlined in this report is for only a simplified two-dimensional geometry as demonstrated in Fig. 3. Zero net diffusion is assumed along the length of the stripes, so

the z dimension can be eliminated from this analysis. The two-dimensional version of Fick's diffusion law is applied to the simulation cell, and the concentration profiles for each metalorganic reactant are calculated with a computer-based finite element solver [30].

The diffusion and reaction characteristics are different for each metalorganic source, so SAE affects not only the growth rate but also the composition of ternary alloys consisting of multiple column III atoms [27]–[29]. The thickness and composition of ternary QW's can be engineered by the SiO_2 growth mask which enables tailoring of effective energy bandgaps across an entire substrate. To model ternary SAE, growth rate enhancement profiles, $E(x)$, are derived for each column III source, and this enhancement data is inserted into the following equations to calculate the profiles of the thickness, $t(x)$, and indium composition, $c(x)$. The nonselective thickness and indium composition targets are noted as t_o and c_o, respectively.

$$t(x) = \{E_{\mathrm{TMIn}}(x) \cdot c_o + E_{\mathrm{TMGa}}(x) \cdot [1 - c_o]\} \cdot t_o \quad (1)$$

$$c(x) = \frac{E_{\mathrm{TMIn}}(x) \cdot c_o}{E_{\mathrm{TMIn}}(x) \cdot c_o + E_{\mathrm{TMGa}}(x) \cdot [1 - c_o]}. \quad (2)$$

Empirical values for the reaction parameters δ and D/k are required for each metalorganic reactant and reactor configuration to accurately predict enhancement profiles. The trimethylgallium (TMGa) and trimethylindium (TMIn) parameters are found through selective growth thickness profiles of the binary compounds GaAs and InP, respectively. Self-consistent solutions to the reaction parameters are found using two different SiO_2 window widths of 50 and 125 μm. After defining the windows and removing the processing damage, the appropriate material is deposited by selective-area atmospheric pressure MOCVD. After growth, the SiO_2 is removed, and the thickness profiles are measured using surface profilometry [31], [32].

As seen in Fig. 4, accurate predictions are obtained for thickness profiles of InGaAs grown on InP ($t_o = 250$ Å, $c_o = 53\%$) [31] and InGaP grown on GaAs ($t_o = 262$ Å, $c_o = 48\%$) [32]. These two ternary growths were performed with different gas velocities and reaction chamber sizes. The TMIn (TMGa) parameters are found using the phosphorous- (arsenic-) based compound InP (GaAs), but the arsenic- (phosphorous-) based compound InGaAs (InGaP) is modeled accurately using these values. Thus, selective growth enhancement is not dependent on the column V reactant [31], [32]. These data support the validity of the SAE model and verify the dominance of gas phase diffusion on growth rate enhancement during selective-area MOCVD.

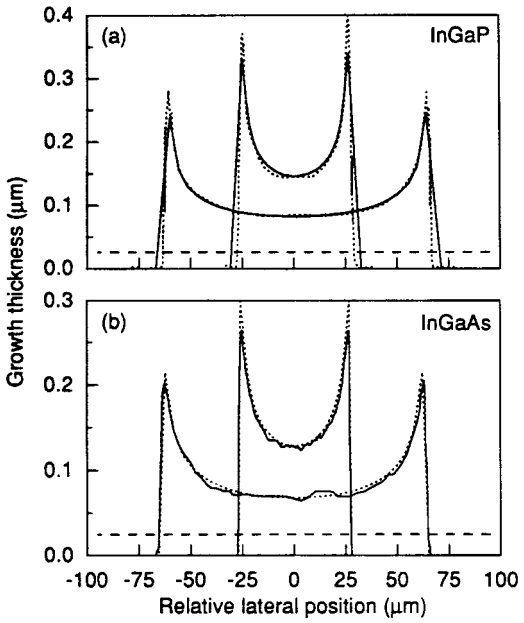

Fig. 4. Measured (solid line) and predicted (dotted line) growth thickness profiles of (a) InGaP on GaAs and (b) InGaAs on InP by selective-area MOCVD. The dashed lines represent the nonselective growth thickness, t_o.

IV. Discrete BH Lasers

BH lasers are desirable because of the strong index guiding and current confinement provided by the heterostructure discontinuity in the lateral direction. These features allow BH lasers to operate with low threshold currents and high efficiencies. Impurity-induced layer disordering (IILD) has been used to fabricate low threshold BH lasers [33], [34], but this technique has the disadvantage of a long anneal at high temperatures which can lead to interdiffusion at the InGaAs-GaAs interface. Low threshold BH lasers have also been grown on nonplanar substrates [35]. This method can produce narrow as-grown active region widths, but the final structure is nonplanar with deep grooves (>2 μm) which can cause subsequent processing problems. The three-step SAE process eliminates much of the difficulty associated with regrowth over exposed AlGaAs.

Selective-area growth utilizing a patterned silicon dioxide mask was used to fabricate the strained-layer InGaAs–GaAs–AlGaAs SQW BH lasers. Regrown interfaces, which increase the electrical and optical losses in a laser heterostructure, are unavoidable in this three-step process. These additional losses lead to a 10%–25% increase in threshold current density [36], but surface preparation techniques proir to regrowth can decrease this effect. The chemical solution used for the surface preparation is of utmost importance in the SAE process. Initially, a H_2SO_4–H_2O_2–H_2O (1:8:80) solution was used to etch back the exposed crystal just prior to regrowth. This process produced lasers with thresholds as low as 10.5 mA and pulsed optical powers as high as 200 mW [13]. The emission wavelength versus oxide stripe width for 4-μm-wide BH mesa devices are shown in Fig. 5. Laser emission wavelengths range from 0.965 to 1.06 μm for variation of oxide widths between 3 and 25 μm. The measured wavelengths are consistent with expected values considering the effects of strain, quantum confinement, and SAE growth rate enhancement.

The H_2SO_4–H_2O_2–H_2O wet etch process prior to regrowth resulted in rough growth surfaces and poor thickness control of the residual GaAs layers on either side of the mesa. Both factors produced large variations in the threshold currents of the SAE devices [13]. Since the processing steps used to fabricate the SAE devices contaminate but not significantly

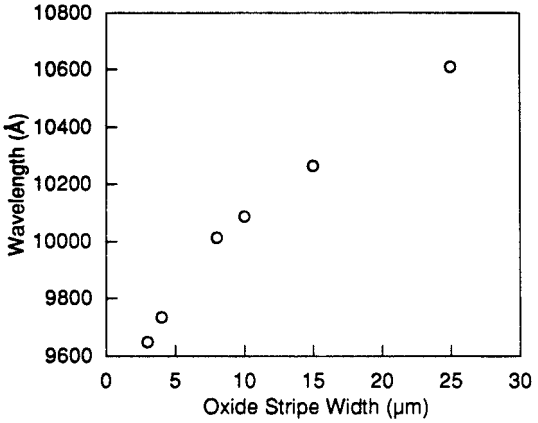

Fig. 5. Wavelength versus oxide stripe width for the selectively grown BH lasers. Wavelengths range from 0.965 μm to 1.06 μm for oxide widths from 3 μm to 25 μm. The measured wavelengths are consistent with values expected considering the effects of strain, quantum confinement, and SAE enhancement.

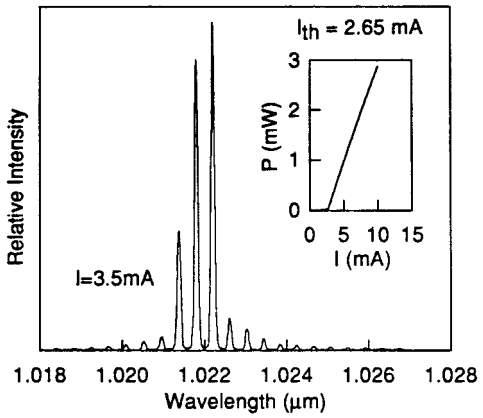

Fig. 6. Longitudinal mode spectrum and power output versus current (inset) of a three-step SAE BH laser with as-cleaved facets operating pulsed at room temperature ($\lambda_{\rm peak} = 1.022$ μm, $I_{\rm th} = 2.65$ mA).

damage the crystalline surface, a surface preparation which does not etch the crystal is more desirable. Using a solution of H_2SO_4–H_2O (1:80), one can remove the surface native oxides without etching the crystal. This not only enables the surface to be extremely smooth but also allows the crystalline layer thickness to be defined solely by the growth and not by the surface preparation etch. Precise thickness control is important for the residual GaAs layers located on either side of the BH mesa because the thinner the residual GaAs layers, the larger the lateral optical confinement and lateral current confinement.

The three-step growth process using the H_2SO_4–H_2O surface preparation [37] begins with the growth of a buffer layer, a 1-μm $Al_{0.60}Ga_{0.40}As$ lower cladding ($T_g = 800$ °C) and a thin (150 Å) GaAs layer to prevent oxidation. The sample is removed from the chamber, and a 600-Å SiO_2 mask is deposited on the sample and patterned by standard lithographic methods. For the 2-μm-wide BH lasers described in this section, the dual oxide stripe widths are 14.5 μm each. An H_2SO_4–H_2O (1:80) etch is used to remove process contamination before the sample is returned to the reactor for the selective growth of the active region. The lower and upper GaAs barriers have thicknesses of 1020 and 2120 Å, respectively, and the InGaAs QW ($T_g = 625$ °C) has a thickness of 94 Å and an indium composition of 24%. The oxide mask is then removed, and another H_2SO_4–H_2O (1:80) etch is performed prior to the final growth, consisting of a 50-Å GaAs layer, a 1-μm $Al_{0.60}Ga_{0.40}As$ upper cladding layer ($T_g = 800$ °C), and a 0.15-μm GaAs p^+ cap ($T_g = 650$ °C). The design of the BH's optimized the optical confinement of the lateral mode. The residual 200-Å of GaAs on each side of the BH mesa raises the effective index in this region only slightly above the index of bulk $Al_{0.60}Ga_{0.40}As$, leaving the lateral optical confinement largely unaffected.

Fig. 6 shows the longitudinal mode spectrum of a 330-μm-long BH laser ($\lambda_{\rm peak} = 1.022$ μm) with as-cleaved facets. The inset of Fig. 6 shows the light versus current (*L–I*) characteristic of this device. A pulsed threshold current of 2.65 mA (401 A/cm^2) and a differential slope efficiency of 0.392 W/A per facet were observed from this device which had an

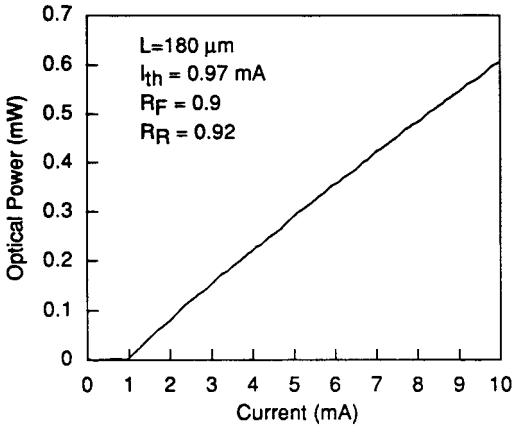

Fig. 7. Pulsed output versus current at low-current levels for one facet of a three-step SAE BH laser ($I_{\rm th} = 0.97$ mA, length 180 μm, active region stripe width 2 μm).

effective lateral index step of 0.19. With the application of HR coatings, a submilliampere (0.97 mA) pulsed threshold current is obtained with a similar 180-μm-long laser, shown in Fig. 7. Peak optical powers of 170 mW/facet are obtained from a 760-μm-long 4-μm-wide BH driven to higher currents. The peak optical power of 170 mW/facet is limited by the onset of catastrophic optical mirror damage (COMD).

V. Integrated BH Devices

A. Lasers with Integrated Electroabsorption Modulators

Electroabsorption (EA) modulators which operate using the quantum-confined Stark effect (QCSE) have been shown to be important components for multigigabit transmission [38]. Discrete EA modulators have also been demonstrated with high extinction ratios (>15 dB) at low biases (<3 V) [38], [39]. Unfortunately, there are many inherent problems associated with using these discrete devices. These problems include insertion loss (typically >3 dB), intracavity reflections, and the need for large optical components for external coupling. Monolithic integration of a laser diode with the EA modulator solves many problems of using multiple discrete devices. In

addition, the compactness of the integrated device results in lower packaging costs.

The fabrication of monolithically integrated modulators which are low loss when unbiased requires that the quantum-confined-state wavelength in the modulator section be blue shifted with respect to the lasing wavelength. One method to obtain this blue shift is by growth on nonplanar substrates [40]. This method has the advantage of only requiring a one step epitaxial growth, but the final structure is usually very nonplanar with deep groves (>1 μm). Another method to produce a blue shift entails removing the active region and regrowing higher bandgap material [41]. This method allows for large bandgap differences between the laser and the modulator, but precise growth control is required to match the waveguides and to prevent coupled-cavity effects between the sections. A third method to form integrated waveguides involves disordering of the QW [42], [43], but this method usually produces QW's with relatively large transition linewidths.

Recently, laser diodes with monolithically integrated EA modulators fabricated using SAE in the InGaAs–InGaAsP material system have received much attention for applications in long-distance fiber communication [44]–[46]. These devices exhibit extinction ratios up to 16 dB for an applied reverse bias of 2 V and over 10-GHz modulation with a voltage swing of 1 V_{pp}. As of yet, little work has been done on laser diodes with monolithically integrated EA modulators in the InGaAs–GaAs material system that has compatibility to GaAs VLSI technology. Applications for these devices include backplane optical interconnections and local area networks [47].

Intracavity Modulators: Fig. 8 is the schematic diagram of a laser with a monolithically integrated intracavity modulator fabricated by SAE. Each device is composed of a gain section and a modulator section separated by a 50 μm wide trench. The devices employ a single QW BH configuration formed by the three-step selective-area MOCVD growth [13], [37]. The laser structure in the gain section consists of a 0.15-μm GaAs:n buffer layer, a 1-μm $Al_{0.60}Ga_{0.40}As$ lower cladding layer, a 1300-Å GaAs lower barrier layer, a 100-Å $In_{0.28}Ga_{0.72}As$ QW, a 1200-Å GaAs upper barrier layer, a 1-μm $Al_{0.60}Ga_{0.40}As$ upper cladding layer, and a 0.1-μm GaAs:p^+ contact layer grown on a GaAs:n substrate. To reduce the lateral current spreading, the sample was etched in H_2SO_4–H_2O_2(30%)–H_2O (1:8:80) for 100 s (etch depth $\sim$0.75 μm) to form a 15-μm mesa centered above the BH mesa. This etch also forms the 50-μm wide 0.75-μm deep trench providing an isolation resistance of >1.5 kΩ between the gain and the modulator sections.

The geometry of the SiO_2 mask used during the selective growth of the active region is a symmetric dual stripe geometry. The spacing between the dual oxide stripes was 5 μm along the entire device, which defines the BH mesa width. The oxide stripe widths in the gain section and the modulator section are 24 and 18 μm, respectively, resulting in emission wavelengths of 1.072 and 1.05 μm, respectively. Thus, the modulator quantum-confined-state wavelength is blue shifted by $\sim$200 Å with respect to the quantum-confined-state wavelength of the gain section, causing the lasing wavelength to be just outside the absorption edge of the unbiased modulator. This allows the unbiased modulator to be transparent to the light generated in the gain section while only a small reverse bias across the modulator is required to shift the absorption edge of the modulator into the lasing wavelength. Operating at small voltages is an important feature of EA modulators due to the absorption peak at the absorption edge decreasing with increasing bias.

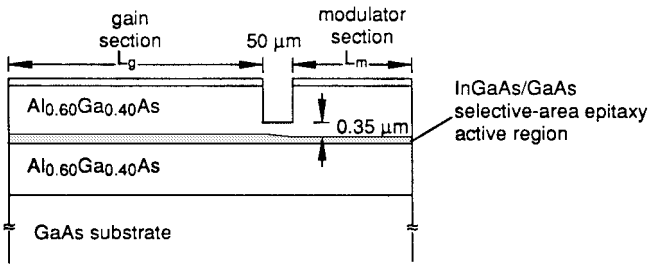

Fig. 8. Schematic diagram of a three-step SAE laser with monolithically integrated intracavity loss modulator.

Fig. 9 shows the continuous-wave (CW) output power exiting the modulator section versus gain section current for different modulator biases for an uncoated device with a 500-μm-long gain section and a 290-μm-long modulator section. The device has a threshold current of 9 mA for a modulator bias of 0 V. This figure shows that a bias of only 2 V across the modulator section terminates the lasing of the device for a gain section current of 25 mA. The static modulation properties for three uncoated devices with gain section lengths of 500 μm and modulator section lengths of 290, 620, and 1020 μm were measured. The gain section of all three devices are biased to produce 5 mW of optical power at a modulator bias of 0 V. Extinction ratios of 16.5, 19.5, and 20.5 dB are observed for devices with modulator biases of 2 V and modulator section lengths of 290, 620, and 1020 μm, respectively. The CW threshold currents are 9.0, 7.5, and 7.5 mA for devices with a modulator bias of 0 V and modulator section lengths of 290, 620, and 1020 μm, respectively. These low-threshold currents show the very low loss of the unbiased modulator as well as the efficient optical coupling between the gain and the modulator sections. From the external differential efficiencies measured at both facets, an optical coupling coefficient of $\sim$90% is calculated [48], [49]. Because of the low absorption by the QW in the unbiased modulator section, the optical loss in the unbiased modulator section is approximately equal to the internal loss ($\alpha_i = 8$ cm^{-1}) obtained from external differential efficiency versus cavity length measurements.

External Cavity Modulators: Wavelength tunable asymmetric cladding ridge waveguide distributed Bragg reflector (DBR) lasers with linewidths as low as 36 kHz have previously been fabricated using an anisotropic grating etch into the upper cladding [50]. These devices exhibit threshold currents as low as 9 mA and slope efficiencies as high as 0.3 W/A. We employ this grating etch along with SAE to fabricate multiple-quantum-well (MQW) wavelength tunable DBR lasers with nonabsorbing gratings and monolithically integrated external cavity EA modulators.

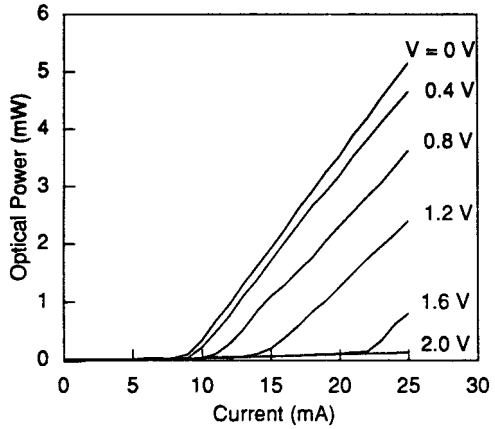

Fig. 9. CW output power exiting the modulator section versus gain section current for various modulator biases.

Fig. 10(a) is the schematic diagram of a MQW wavelength-tunable DBR laser with monolithically integrated external cavity EA modulator. These devices employ a BH configuration formed by a three-step selective-area growth process [13], [37]. The laser structure consists of a GaAs:n buffer layer, a 1-μm $Al_{0.60}Ga_{0.40}As$ lower cladding layer, an 860-Å GaAs lower guide layer, three 85-Å $In_{0.24}Ga_{0.76}As$ QW's separated by two 110-Å GaAs barriers, a 960-Å GaAs upper guide layer, a 0.4-μm $Al_{0.60}Ga_{0.40}As$ upper cladding layer, and a 0.1-μm GaAs:p^+ contact layer. To reduce the lateral current spreading as well as lower the parasitic capacitance, the sample was etched in H_2SO_4–H_2O_2(30%)–H_2O (1:8:80) forming a 15-μm-wide 0.6-μm-deep mesa centered above the BH mesa. Second-order DBR gratings were formed by electron beam lithography and reactive ion etching [50]. The gratings have a 30% duty cycle, a 0.309-μm period, and a 0.215-μm etch depth. The gratings are 100-μm long and 50-μm wide to span the entire etched mesa width. A 4-μm wide contact window was then opened above the BH mesa along the entire device. P-side metals consisting of Ti–Pt–Au (15-Å–15-Å–1500-Å) [51] were deposited and patterned using a liftoff process to provide separate contact pads to the laser, DBR, and modulator sections. The pad separation is 15 μm, centered over the edge of the DBR grating [see Fig. 10(a)] and allows the grating etch to serve as isolation between the DBR grating and the laser, and between the DBR grating and the modulator. The sample was thinned to $\sim$120 μm before the n-side metals (Ge–Au) were deposited and alloyed. The sample was cleaved into bars to finish the processing.

Fig. 10(b) is the schematic diagram of the dual oxide stripe mask used during the selective growth of the active region for the device shown in Fig. 10(a). The distance between the stripes is 4 μm which defines the BH mesa width. Each oxide stripe is 12 μm wide in the modulator and widens in the DBR laser to 16 μm, resulting in quantum-confined-state wavelengths of $\lambda_M = 0.999$ μm and $\lambda_{\mathrm{LD}} = 1.026$ μm for the modulator and the laser, respectively. Thus, the wavelength tunability of SAE is used to blue shift the modulator quantum-confined-state wavelength by $\sim$250 Å with respect to the quantum-confined-state wavelength of the laser. The asymmetric growth mask produces a tapered active

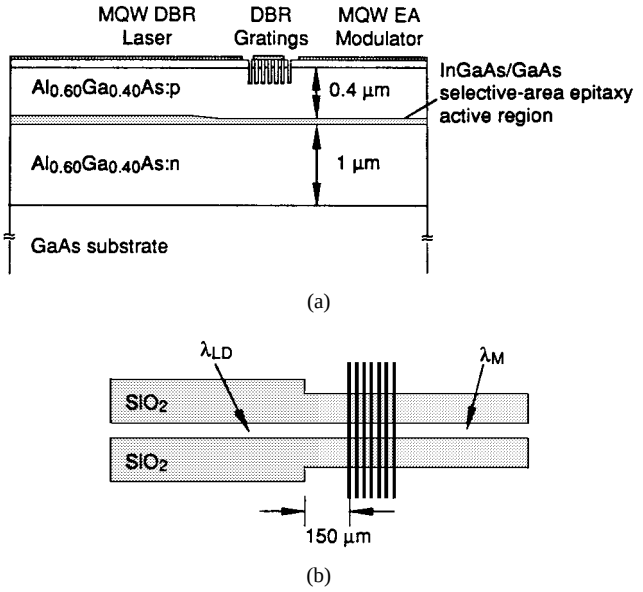

Fig. 10. (a) Schematic diagram of a MQW wavelength-tunable DBR laser with monolithically integrated external cavity EA modulator. (b) Schematic diagram of the dual oxide stripe mask used during the selective growth of the active region for the device shown in Fig. 10(a).

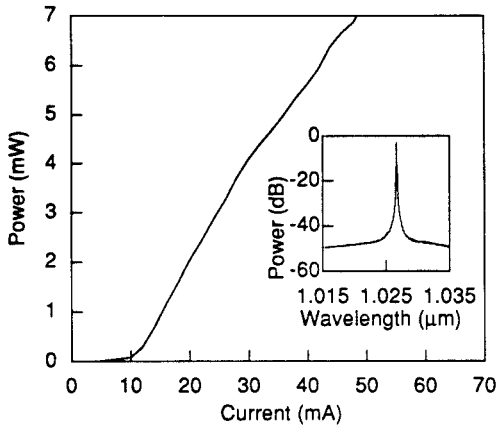

Fig. 11. CW output power from the cleaved laser facet versus laser current for an uncoated monolithically integrated DBR laser/modulator. Inset: longitudinal mode spectrum for the same device at a CW laser current of $2 \times I_{\mathrm{th}}$.

region thickness, and thus a tapered effective index, near the discontinuity in the oxide width. To prevent the DBR grating from being highly chirped, the DBR gratings are positioned 150 μm away from the change in oxide width [see Fig. 10(b)] where the active region thickness is relatively constant (change in active region thickness across the DBR section is calculated to be 0.62% [31]). This positioning of the DBR grating also enables the DBR grating to be nonabsorbing to the laser light.

Fig. 11 shows the CW optical output power from the cleaved laser facet versus laser current for an uncoated device with a 700-μm-long laser, a 100-μm-long DBR grating, and a 490-μm-long modulator. The device has a CW threshold current of 10.5 mA ($J_{\mathrm{th}} = 375$ A/cm^2) and a slope efficiency of 0.21 W/A. For comparison, Fabry–Perot lasers fabricated from the same selectively grown material exhibit similar CW threshold currents ($\sim$11 mA) and similar slope efficiencies

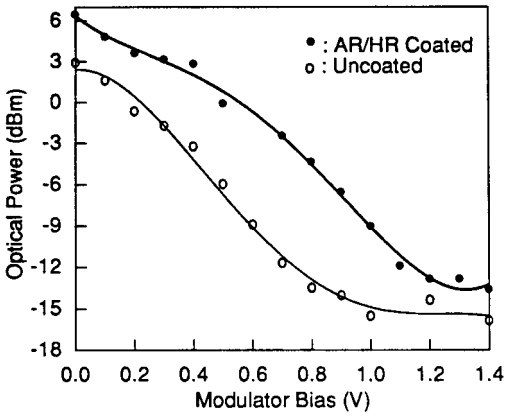

Fig. 12. CW output power, measured with a broad-area detector, exiting the modulator facet versus modulator bias for the same device tested in Fig. 11. The device was tested with uncoated facets, as well as with HR/AR coated facets.

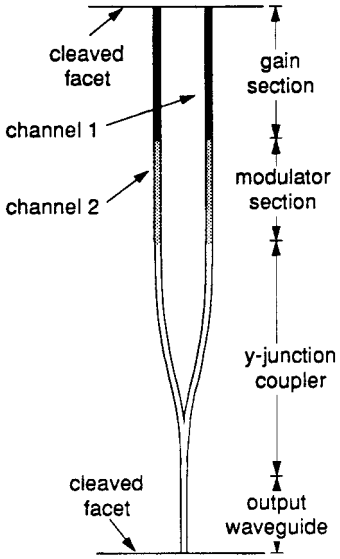

Fig. 13. Schematic diagram of a dual wavelength source with monolithically integrated EA modulators by selective-area MOCVD. The lengths of the gain and modulator sections are 800 and 400 μm, respectively, and the radius of the y-junction s-bends is 400 μm.

($\sim$0.2 W/A). The inset of Fig. 11 shows the longitudinal mode spectrum of the same device at a CW laser current of $2 \times I_{\rm th}$. The peak emission wavelength is 1.027 μm with a SMS ratio of $>$40 dB. Many devices tested exhibit two or three dominate emission wavelength peaks. We believe this is a result of the 4-μm-wide devices operating with multilateral modes where each lateral mode propagates with a slightly different effective index [52]. Wavelength tuning of 7 nm is obtained by injection current heating of the DBR section with a DBR section current of 60 mA.

Fig. 12 shows the CW output power, measured with a broad-area detector, exiting the modulator facet versus modulator bias for the same device tested in Fig. 11. All results were obtained with an unbiased DBR grating. The device was tested with uncoated facets, as well as with HR $(R \sim 95\%)$ and AR $(R \sim 2.5\%)$ coatings deposited on the laser and the modulator facet, respectively. The isolation resistance between the laser and the modulator is 6.0 kΩ. The uncoated device (HR/AR coated device) operated with a CW laser bias of 50 mA (40 mA) and exhibited an extinction ratio of 18 dB (18 dB) for a low modulator bias of 1 V (1.1 V). The extinction ratio saturating at $\sim$18 dB in Fig. 12 is the result of optical scattering at the active region thickness taper as well as surface emission at the second-order DBR grating impinging on the broad-area detector. When coupled to a singlemode fiber the extinction ratio for the HR/AR coated device increased to 22 dB for a modulator bias of 1 V and saturated at 40 dB with a modulator bias of 1.25 V. These fiber coupled results were obtained with a CW laser bias of 40 mA. The L–I characteristics from the cleaved laser facet show only a 60-μW decrease in optical output power when the modulator bias is increased from 0 to 1.5 V. This slight decrease in output power is the result of 0.25 mA of leakage current through the laser at a modulator bias of 1.5 V.

B. Dual Wavelength Source

Multiple wavelength laser sources are of considerable importance for a variety of applications, including optical color printing [53], WDM [54], and remote sensing by differential absorption measurements [55]. Several recent studies have shown successful fabrication of such sources [22], [56], [57]; however, many rely on a large spatial separation between elements, and therefore complex focusing optics are required to align the individual lasers to optical fiber links. By combining the optical signals monolithically on a wafer, the alignment restrictions can be eliminated. Lammert *et al.* have recently reported a dual wavelength source with monolithically integrated waveguide coupler fabricated by three-step selective-area MOCVD [58]. In this design, two distinct wavelength sources (channels) are guided into two closely spaced s-bend transition waveguides that are separated at the output facet by 2 μm. This small separation allows relatively efficient coupling of the two channels into a single mode fiber. For larger channel densities, however, the coupling efficiency for the outer channels dramatically decreases as a result of misalignment of the lateral mode with the optical lens system [59], [60]; accordingly, monolithic integration of a single output waveguide is preferred. The introduction of a y-junction coupler into the above design appears to be the simplest approach; however, optical crosstalk between the channels prevents independent operation of the two sources. For relatively small biases applied to the high energy device, the low energy device is optically pumped above threshold. As a result, both diodes operate simultaneously when only one is pumped. By monolithically integrating an EA modulator into each cavity to provide a voltage controllable loss, independent and simultaneous laser operation can be obtained with a y-junction coupler configuration. In this section, we present the design, fabrication, and results of a dual wavelength source with monolithically integrated EA modulators and y-junction coupler by selective-area MOCVD.

Fig. 13 shows a schematic diagram of the dual wavelength laser devices. Each device is separated by 125 μm and contains four sections: a gain section, a modulator section, a y-junction

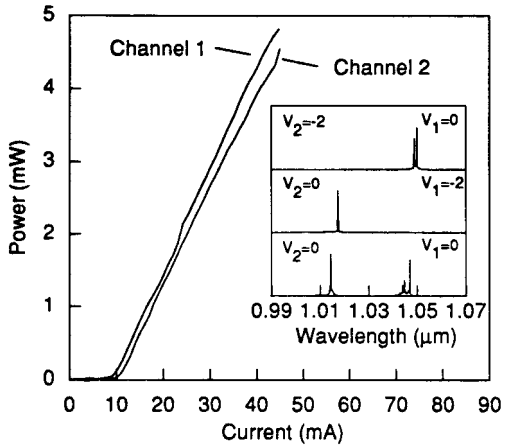

Fig. 14. L–I characteristics for a dual-channel source operating CW at room temperature. The threshold current for channel 1 (channel 2) is 9.5 mA (10.1 mA). The inset shows the longitudinal mode spectra for the two channels biased simultaneously at 15 mA with the indicated voltage applied to the modulator sections.

coupler, and an output waveguide. The gain and modulator sections form the active elements in the cavity, while the passive y-junction coupler is used to direct the two signals into a single output waveguide. The length of the gain and modulator sections for each device is 800 and 400 μm, respectively. The radius of curvature of the y-junction s-bends is 400 μm. Due to the strong lateral index guiding in the BH configuration, the bend loss in the y-junction waveguides is small [61]. In addition, the passive y-junction coupler is designed to have a thinner QW than the gain and modulator sections and therefore is transparent to the light generated in either section. Electrical isolation between the laser and modulator was obtained by etching through the GaAs cap layer (and into the AlGaAs cladding) between the laser and modulator sections. This 50-μm-long, 0.7-μm-deep trench provides an isolation resistance of $\sim$1.2 kΩ. Another deeper etch was performed in the region between the two channels to provide a 7.5-kΩ resistance between each channel. Finally, a liftoff process was used to define separate p-contact metal pads to the individual sections.

Two distinct laser emission wavelengths were obtained for the two channels by incorporating different oxide mask widths in the gain regions. The width of the BH (4 μm) is constant along the enitre length of the device, and the oxide stripe widths were designed to produce peak emission wavelengths at 1.045 μm (1.025 μm) and 1.017 μm (1.001 μm) for the gain and modulator sections of channel 1 (channel 2), respectively. The modulator for each channel has a quantum-confined energy state that is blue shifted with respect to the $n = 1$ optical transition of the gain section to insure that each unbiased modulator is transparent to the light generated in its corresponding gain region. The QCSE is used to shift the absorption edge of the modulator into the lasing wavelength of the gain section thereby introducing a voltage-controllable loss into the cavity.

The devices were tested for light output power versus current characteristics and spectra. Fig. 14 shows the CW L–I characteristics for the two channels biased independently. The threshold current value for channel 1 and channel 2 is 9.5 mA and 10.1 mA, respectively. The inset of Fig. 14 shows the CW longitudinal mode spectra from the same device under different operating conditions. The three spectra were measured with a 15 mA driving current applied to the gain section of each channel. Each channel was simultaneously coupled into a single mode fiber, and the spectra were measured using an optical spectrum analyzer. The lower spectrum, in Fig. 14, shows channel 1 and channel 2 operating simultaneously with modulator biases of 0 V, while the upper spectra show channel 1 "on" and channel 2 "off" and visa-versa. The "off" state in both cases is achieved by applying a modulator bias of -2 V. A slight red shift of approximately 4 nm is observed in the upper spectra as a result of junction heating from the photogenerated current.

C. Broad Spectrum Edge Emitting LEDs

LED's and superluminescent diodes (SLD's) with broad spectral width [62], [63] are attractive light sources for a number of applications, including fiber-optic gyroscopes and sources used in conjunction with spectroscopic elements in remote sensing applications. The fabrication of edge emitting LED devices is usually based on the separate confinement heterostructure laser design with the addition of a lossy region to inhibit feedback in the cavity and thus suppress lasing. Since the light emitted from these devices consists of spontaneous radiation, the spectral width and appearance of the emission pattern will resemble the gain spectrum. With single QW structures, however, the width of the gain spectrum, for a single $n = 1$ transition, is limited by both the source wavelength $(\Delta\lambda \propto \lambda^2)$ [64] and the active region material used. Therefore, in order to increase the spectral bandwidth of the device, it is necessary to fabricate a structure which will broaden the net optical gain spectrum. Several recent studies have shown a broadening of the gain spectrum, and thus the spectral width of the emission, by control of the active region design. A number of approaches have been implemented, including the use of stacked active layers and multiple asymmetric QW's [65]–[67]. Our approach to the problem is to increase the width of the optical gain spectrum by varying the QW thickness along the length of the device, in order to provide additional broadening to the single QW gain profile. In this section, we demonstrate an InGaAs–GaAs–AlGaAs single QW broad-spectrum LED by selective-area MOCVD. This device utilizes both a continuous variation in QW thickness to produce broadband emission and a rear absorber configuration to suppress lasing.

Fig. 15 shows the mask pattern used to define the selective growth of the active region. The spacing between the stripes defines the lateral dimension of the emitter, and the width of the stripes at any point defines the quantum-confined-energy state at that point. The tapered region is pumped to produce a broadband of light emission, and the constant width dual oxide stripe section, which has a lower quantum-confined-energy state than the light produced in the tapered region, acts as an absorber to suppress lasing. The basis of the LED structure is the tapered oxide mask region. The variation in oxide width

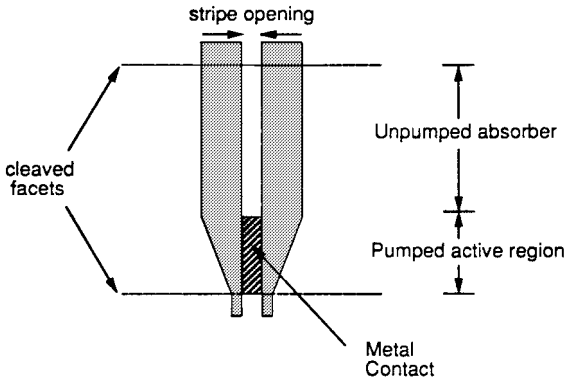

Fig. 15. Mask used to define the selective growth of the LED device. The tapered section defines the pumped gain region, while the symmetric stripes form the unpumped absorber. The lengths of the pumped and unpumped regions are 200 and 500 μm, respectively.

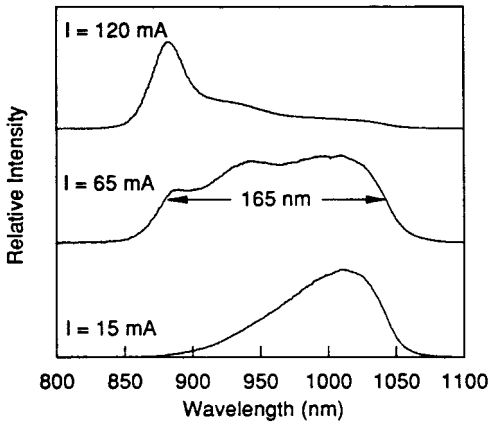

Fig. 16. Spectra of a 10 μm wide LED tested at 15, 65, and 120 mA under pulsed conditions. The above spectra were measured with a spectrometer resolution of 1.5 nm.

is designed to provide enough growth rate enhancement, and corresponding composition variation, along the length of the stripe to produce a large spectral range of light emission while simultaneously insuring that the maximum QW thickness is below critical thickness. All of the devices fabricated have either a 4- or 10-μm stripe opening and are 700 μm in length. The lengths of the pumped and unpumped regions are 200 and 500 μm, respectively. The oxide width, in the pumped region, is linearly tapered from 2 μm at the narrow end to 25 and 50 μm at the wide end for the 4- and 10-μm stripe openings, respectively, to take full advantage of the broad tuning range available with the selective growth process.

The devices were tested for light output power versus current characteristics and spectra. Shown in Fig. 16 are the output spectra from a 10-μm-wide LED device tested at several different pumping levels. At relatively low injection currents, the emission from the LED exhibits a broad spectral width of 84 nm centered at 1.0 μm with the spectral linewidth of the emitted light determined by the net gain profile of the tapered QW. As the injected current is increased, second state emission from the InGaAs QW becomes evident in the spectrum until the emission from the QW saturates, and the carriers leak out into the GaAs barriers and undergo recombination at shorter emission wavelengths. The optical spectrum at this pumping level displays a broad spectral linewidth of 165 nm. At higher pumping levels, emission from the bulk GaAs, centered at 890 nm, dominates the spectral appearance of the light emitted. The devices fabricated in this work showed evidence of second state emission at relatively low injection currents due to the short length of the pumped QW region. By further optimizing the pumped active region, the authors anticipate that the output power, and spectral bandwidth can be maximized to achieve peak device performance.

VI. Conclusion

Selective-area MOCVD technology has been reviewed, and progress toward photonic applications has been discussed. The behavior of selective-area growth is simulated with a computational diffusion model, and accurate predictions for the thickness and composition of selectively grown ternary compounds are obtained. High-performance results have been presented from BH devices involving SAE during the deposition of their active regions. These include low-threshold BH lasers, laser diodes integrated with either intracavity or external cavity modulators, dual-channel emitters integrated with both modulators and passive y-junction waveguides, and broadband LED's. The performance of these devices demonstrates the utility of selective-area MOCVD in the fabrication of future photonic integrated circuits.

Acknowledgment

The authors recognize T. M. Cockerill, J. A. Dantzig, D. E. Ackley, J. H. Hughes, J. F. Kluender, G. M. Smith, and D. V. Forbes for contributions.

References

[1] P. K. York, K. J. Beernink, G. E. Fernández, and J. J. Coleman, "InGaAs-GaAs strained-layer quantum well buried heterostructure lasers ($\lambda > 1$ μm) by metalorganic chemical vapor deposition," *Appl. Phys. Lett.*, vol. 54, pp. 499–501, 1989.

[2] T. Tsukada, "GaAs-$Ga_{1-x}Al_xAs$ buried-heterostructure injection lasers," *J. Appl. Phys.*, vol. 45, pp. 4899–4906, 1974.

[3] B. Zhao, T. R. Chen, Y. H. Zhuang, and A. Yariv, "High speed operation of very low threshold strained InGaAs/GaAs double quantum well lasers," *Appl. Phys. Lett.*, vol. 60, pp. 1295–1297, 1992.

[4] T. R. Chen, L. Eng, B. Zhao, Y. H. Zhuang, S. Sanders, H. Morkoc, and A. Yariv, "Submilliamp threshold InGaAs-GaAs strained layer quantum-well laser," *IEEE J. Quantum Electron.*, vol. 26, pp. 1183–1190, 1990.

[5] J. W. Xiao, J. Y. Xu, G. W. Yang, J. M. Zhang, Z. T. Xu, and L. H. Chen, "Extremely low threshold current, buried-heterostructure strained InGaAs-GaAs multiquantum well lasers," *Electron. Lett.*, vol. 28, pp. 154–157, 1992.

[6] D. C. Liou, W. H. Chiang, C. P. Lee, K. H. Chang, D. G. Liu, J. S. Wu, and Y. K. Tu, "A novel technique for low-threshold and high-power InGaAs/GaAs strained-layer 0.98-μm buried heterostructure laser fabrication," *J. Appl. Phys.*, vol. 71, pp. 1525–1527, 1992.

[7] N. Chand, N. K. Dutta, and S. N. G. Chu, "High performance strained InGaAs/AlGaAs buried-heterostructure quantum-well lasers fabricated by in situ etching and regrowth," *Appl. Phys. Lett.*, vol. 62, pp. 1818–1820, 1993.

[8] J. S. Major, Jr., L. J. Guido, K. C. Hsieh, N. Holonyak Jr., W. Stutius, P. Gavrilovic, and J. E. Williams, "Low-threshold disorder-defined buried heterostructure strained-layer $Al_yGa_{1-y}As$-GaAs-$In_xGa_{1-x}As$ quantum well lasers," *Appl. Phys. Lett.*, vol. 54, pp. 913–915, 1989.

[9] J. Lopata, N. K. Dutta, W. S. Hobson, and P. R. Berger, "Buried heterostructure lasers using a single-step metalorganic chemical vapor deposition growth over patterned substrates," in *Proc. SPIE*, 1992, vol. 1676, pp. 117–121.

[10] T. M. Cockerill, D. V. Forbes, H. Han, B. A. Turkut, J. A. Dantzig, I. M. Robertson, and J. J. Coleman, "Wavelength tuning in strained-layer InGaAs-GaAs-AlGaAs quantum well lasers by selective-area MOCVD," *J. Electronic Mater.*, vol. 23, pp. 115–119, 1994.

[11] T. M. Cockerill, D. V. Forbes, H. Han, and J. J Coleman, "Monolithic integration of a strained-layer InGaAs-GaAs-AlGaAs quantum-well laser with a passive waveguide by selective-area MOCVD," *IEEE Photon. Technol. Lett.*, vol. 4, pp. 448–450, 1993.

[12] L. M. Miller and J. J. Coleman, *CRC Crit. Rev. Solid State Mater. Sci.*, vol. 15, pp. 1–26, 1988.

[13] T. M. Cockerill, D. V. Forbes, J. A. Dantzig, and J. J. Coleman, "Strained-layer InGaAs-GaAs-AlGaAs buried-heterostructure quantum-well lasers by three-step selective-area metalorganic chemical vapor deposition," *IEEE J. Quantum Electron.*, vol. 30, pp. 441–445, 1994.

[14] R. Bhat, "Current status of selective area epitaxy by OMCVD," *J. Crystal Growth*, vol. 120, pp. 362–368, 1992.

[15] O. Kayser, "Selective growth of InP/GaInAs in LP-MOVPE and MOMBE/CBE," *J. Cryst. Growth*, vol. 107, pp. 989–998, 1991.

[16] R. M. Lammert, D. V. Forbes, G. M. Smith, M. L. Osowski, and J. J. Coleman, "InGaAs-GaAs quantum-well lasers with monolithically integrated intracavity electroabsorption modulators by selective-area MOCVD," *IEEE Photon. Technol. Lett.*, vol. 8, pp. 78–80, 1996.

[17] R. M. Lammert, G. M. Smith, J. S. Hughes, M. L. Osowski, A. M. Jones, and J. J. Coleman, "MQW wavelength-tunable DBR lasers with monolithically integrated external cavity electroabsorption modulators with low-driving-voltages fabricated by selective-area MOCVD," *IEEE Photon. Technol. Lett.*, vol. 8, pp. 797–799, 1996.

[18] M. Aoki, M. Suzuki, T. Taniwatari, H. Sano, and T. Kawano, "New photonic device integration by selective-area MOVPE and its application to optical modulator/laser integration," *Microwave Opt. Technol. Lett.*, vol. 7, pp. 132–139, 1994.

[19] R. M. Lammert, P. V. Mena, D. V. Forbes, M. L. Osowski, S. M. Kang, and J. J. Coleman, "Strained-layer InGaAs-GaAs-AlGaAs lasers with monolithically integrated photodiodes by selective-area MOCVD," *IEEE Photon. Technol. Lett.*, vol. 7, pp. 247–250, 1995.

[20] M. L. Osowski, T. M. Cockerill, R. M. Lammert, D. V. Forbes, D. E. Ackley, and J. J. Coleman, "A strained-layer InGaAs-GaAs-AlGaAs single quantum well broad spectrum LED by selective-area MOCVD," *IEEE Photon. Technol. Lett.*, vol. 6, pp. 1289–1292, 1994.

[21] M. L. Osowski, R. M. Lammert, D. V. Forbes, D. E. Ackley, and J. J. Coleman, "Broadband emission from InGaAs-GaAs-AlGaAs LED with integrated absorber by selective-area MOCVD," *Electron. Lett.*, vol. 31, pp. 1498–1499, 1995.

[22] T. M. Cockerill, R. M. Lammert, D. V. Forbes, M. L. Osowski, and J. J. Coleman, "Twelve-channel strained-layer InGaAs-GaAs-AlGaAs buried heterostructure quantum well laser array for WDM applications by selective-area MOCVD," *IEEE Photon. Technol. Lett.*, vol. 6, pp. 786–788, 1994.

[23] M. L. Osowski, R. M. Lammert, and J. J. Coleman, "A dual-wavelength source with monolithically integrated electroabsorption modulators and y-junction coupler by selective-area MOCVD," *IEEE Photon. Technol. Lett.*, vol. 9, pp. 158–160, 1997.

[24] T. M. Cockerill, M. L. Osowski, R. M. Lammert, and J. J. Coleman, "A strained-layer InGaAs-GaAs buried heterostructure circular ring laser with integrated y-coupled passive waveguide by selective-area metalorganic chemical vapor deposition," in *Proc. 14th IEEE Int. Semiconduct. Laser Conf.*, 1994, pp. 195–196.

[25] A. R. Clawson, C. M. Hanson, and T. T. Vu, "MOVPE growth of SiO_2-masked InP structures at reduced pressures," *J. Cryst. Growth*, vol. 77, pp. 334–339, 1986.

[26] K. Yamaguchi, M. Ogasawara, and K. Okamoto, "Surface-diffusion model in selective metalorganic chemical vapor deposition," *J. Appl. Phys.*, vol. 72, pp. 5919–5925, 1991.

[27] K. Yamaguchi and K. Okamoto, "Lateral supply mechanisms in selective metalorganic chemical vapor deposition," *Jpn. J. Appl. Phys.*, vol. 32, pp. 1523–1527, 1993.

[28] C. Caneau, R. Bhat, M. R. Frei, C. C. Chang, R. J. Deri, and M. A. Koza, "Studies on the selective OMVPE of (Ga, In)/(As, P)," *J. Cryst. Growth*, vol. 124, pp. 243–248, 1992.

[29] J. Finders, J. Geurts, A. Kohl, M. Weyers, B. Opitz, O. Kayser, and P. Balk, "Composition of selectively grown $In_xGa_{1-x}As$ structures from locally resolved raman spectroscopy," *J. Cryst. Growth*, vol. 107, pp. 151–155, 1991.

[30] "FIDAP Fluid Dynamics Analysis Package," version 7.05, Fluid Dynamics International, Inc., Evanston, IL, 1993.

[31] A. M. Jones, M. L. Osowski, R. M. Lammert, J. A. Dantzig, and J. J. Coleman, "Growth, characterization, and modeling of ternary InGaAs-GaAs quantum wells by selective-area metalorganic chemical vapor deposition," *J. Electron. Mater.*, vol. 24, pp. 1631–1636, 1995.

[32] J. F. Kluender, A. M. Jones, R. M. Lammert, J. E. Baker, and J. J. Coleman, "Growth, characterization and modeling of $In_xGa_{1-x}P$ stripes by selective-area MOCVD," *J. Electron. Mater.*, vol. 25, pp. 1514–1520, 1996.

[33] D. G. Deppe, K. C. Hsieh, and N. Holonyak, Jr., "Low-threshold disorder-defined buried-heterostructure AlGaAs-GaAs quantum well lasers," *J. Appl. Phys.*, vol. 58, pp. 4515–4520, 1985.

[34] J. E. Epler, R. L. Thornton, W. J. Mosby, and T. L. Paoli, "Low threshold buried-heterostructure quantum well lasers by excimer laser assisted disordering," *Appl. Phys. Lett.*, vol. 53, pp. 1459–1461, 1988.

[35] K. M. Dzurko, E. P. Menu, C. A. Beyler, J. S. Osinski, and P. D. Dapkus, "Temperature engineered growth of low-threshold quantum well lasers by metalorganic chemical vapor deposition," *Appl. Phys. Lett.*, vol. 54, pp. 105–107, 1989.

[36] T. M. Cockerill, J. Honig, D. V. Forbes, K. J. Beernink, and J. J. Coleman, "Characterization of electrical and optical loss of MOCVD regrowth in strained layer InGaAs-GaAs quantum well heterostructure lasers," *J. Crystal Growth*, vol. 124, pp. 553–557, 1992.

[37] R. M. Lammert, T. M. Cockerill, D. V. Forbes, G. M. Smith, and J. J. Coleman, "Submilliampere threshold buried-heterostructure InGaAs/GaAs single quantum well lasers grown by selective-area epitaxy," *IEEE Photon. Technol. Lett.*, vol. 6, pp. 1073–1075, 1994.

[38] T. Ido, H. Sano, D. J. Moss, S. Tanaka, and A. Takai, "Strained InGaAs/InAlAs MQW electro-absorption modulators with large bandwidth and low driving voltage," *IEEE Photon. Technol. Lett.*, vol. 6, pp. 1207–1209, 1994.

[39] D. Moss, D. Landheer, A. Delage, F. Chatenoud, and M. Dion, "Laser compatible waveguide electroabsorption modulator with high contrast and low operating voltage in GaAs/AlGaAs," *IEEE Photon. Technol. Lett.*, vol. 3, pp. 645–647, 1991.

[40] F. Koyama, K. Y. Liou, A. G. Dentai, G. Raybon, and C. A. Burrus, "GaInAs/GaInAsP strained quantum well monolithic electrabsorption modulator/amplifier by lateral bandgap control with nonplanar substrates," *Electron. Lett.*, vol. 29, pp. 2104–2106, 1993.

[41] K. Sato, K. Wakita, I. Kotaka, Y. Kondo, and M. Yamamoto, "Monolithic strained-InGaAsP multiple-quantum-well lasers with integrated electroabsorption modulators for active mode locking," *Appl. Phys. Lett.*, vol. 65, pp. 1–3, 1994.

[42] S. O'Brien and J. R. Shealy, "Monolithic integration on an (Al)GaAs laser and an intracavity electroabsorption modulator using selective partial interdiffusion," *Appl. Phys. Lett.*, vol. 58, pp. 1363–1365, 1991.

[43] R. L. Thornton, W. J. Mosby, and T. L. Paoli, "Monolithic waveguide coupled cavity lasers and modulators fabricated by impurity induced disordering," *J. Lightwave Technol.*, vol. 6, pp. 786–792, 1988.

[44] M. Aoki, M. Takahashi, M. Suzuki, H. Sano, K. Uomi, T. Kawano, and A. Takai, "High-extinction-ratio MQW electroabsorption-modulator integrated DFB laser fabricated by in-plane bandgap energy control technique," *IEEE Photon. Technol. Lett.*, vol. 4, pp. 580–582, 1992.

[45] T. Kato, T. Sasaki, K. Komatsu, and I. Mito, "DFB-LD/modulator integrated light source by bandgap controlled selective MOVPE," *Electron. Lett.*, vol. 28, pp. 153–154, 1992.

[46] M. Aoki, M. Suzuki, H. Sano, T. Kawano, T. Ido, T. Taniwatari, K. Uomi, and A. Takai, "InGaAs/InGaAsP MQW electroabsorption modulator integrated with a DFB laser fabricated by band-gap energy control selective area MOCVD," *IEEE J. Quantum Electron.*, vol. 29, pp. 2088–2096, 1993.

[47] C. Fan, D. W. Shih, M. W. Hansen, S. C. Esener, and H. H. Wieder, "Quantum-confined stark effect modulators at 1.06 μm on GaAs," *IEEE Photon. Technol. Lett.*, vol. 5, pp. 1383–1385, 1993.

[48] T. Takamori, L. A. Coldren, and J. L. Merz, "Folded-cavity transverse junction stripe surface-emitting laser," *Appl. Phys. Lett.*, vol. 55, pp. 1053–1055, 1989.

[49] R. M. Lammert, G. M. Smith, D. V. Forbes, M. L. Osowski, and J. J. Coleman, "Strained-layer InGaAs-GaAs-AlGaAs buried-heterostructure lasers with nonabsorbing mirrors by selective-area MOCVD," *Electron. Lett.*, vol. 31, pp. 1070–1071, 1995.

[50] G. M. Smith, J. S. Hughes, R. M. Lammert, M. L. Osowski, G. C. Papen, J. T. Verdeyen, and J. J. Coleman, "Very narrow linewidth asymmetric cladding InGaAs-GaAs ridge waveguide DBR lasers," *IEEE Photon. Technol. Lett.*, vol. 8, pp. 476–478, 1996.

[51] G. M. Smith, D. V. Forbes, R. M. Lammert, and J. J. Coleman, "Metallization to asymmetric cladding SCH lasers," in *Proc. SPIE*, 1995, vol. 2613, pp. 107–114.

[52] W. Streifer, D. R. Scifres, and R. D. Burnham, "Analysis of gain-induced waveguiding in stripe geometry diode lasers," *IEEE J. Quantum Electron.*, vol. 14, pp. 418–427, 1978.

[53] K. J. Beernink, R. L. Thornton, and H. F. Chung, "Low threshold current dual wavelength planar buried heterostructure lasers with close spatial and large spectral separation," *Appl. Phys. Lett.*, vol. 64, pp. 1082–1084, 1994.
[54] J. E. Epler, D. W. Treat, S. E. Nelson, and T. L. Paoli, "Multiple wavelength diode laser super array," *IEEE J. Quantum Electron.*, vol. 26, pp. 663–668, 1990.
[55] D. Jacob, N. H. Tran, F. Bretenaker, and A. LeFloch, "Differential absorption measurement of methane with two spectrally resolved laser lines," *Appl. Opt.*, vol. 33, pp. 3261–3264, 1994.
[56] T. Yamada, R. Iga, and H. Sugiura, "Double-wavelength laser array with InGaAsP/InGaAsP multiple quantum well grown by Ar ion laser-assisted metalorganic molecular beam epitaxy," *Appl. Phys. Lett.*, vol. 61, pp. 2449–2451, 1992.
[57] G. P. Li, T. Makino, A. Sarangan, and W. Huang, "16-wavelength gain-coupled DFB laser array with fine tunability," *IEEE Photon. Technol. Lett.*, vol. 8, pp. 22–24, 1996.
[58] R. M. Lammert, T. M. Cockerill, D. V. Forbes, and J. J. Coleman, "Dual-channel strained-layer InGaAs-GaAs-AlGaAs WDM source with integrated coupler by selective-area MOCVD," *IEEE Photon. Technol. Lett.*, vol. 6, pp. 1167–1169, 1994.
[59] H. Sato, M. Aoki, M. Takahashi, M. Komori, K. Uomi, and S. Tsuji, "1.3 μm beam-expander integrated laser grown by single-step MOVPE," *Electron. Lett.*, vol. 31, pp. 1241–1242, 1995.
[60] H. Fukano, Y. Kadota, Y. Kondo, M. Ueki, Y. Sakai, K. Kasaya, K. Yokoyama, and Y. Tohmori, "1.3 μm large spot-size laser diodes with laterally tapered active layer," *Electron. Lett.*, vol. 31, pp. 1439–1440, 1995.
[61] A. Crook, T. M. Cockerill, D. V. Forbes, T. A. DeTemple, and J. J. Coleman, unpublished data.
[62] T. R. Chen, L. Eng, Y. H. Zhuang, A. Yariv, N. S. Kwong, and P. C. Chen, "Quantum well superluminescent diode with very wide emission spectrum," *Appl. Phys. Lett.*, vol. 56, pp. 1345–1346, 1990.
[63] A. T. Semenov, V. K. Batovrin, I. A. Garmash, V. R. Shidlovsky, M. V. Shramenko, and S. D. Yakubovich, "(GaAl)As SQW superluminescent diodes with extremely low coherence length," *Electron. Lett.*, vol. 31, pp. 314–315, 1995.
[64] T. Fukui and Y. Horikoshi, "Anomalous luminescence near the InGaAsP-InP heterojunction interface," *Jpn. J. Appl. Phys.*, vol. 30, pp. 961–965, 1979.
[65] O. Mikami, H. Yasaka, and Y. Noguchi, "Broader spectral width InGaAsP stacked active layer superluminescent diodes," *Appl. Phys. Lett.*, vol. 56, pp. 987–989, 1990.
[66] H. Hager, C. S. Hong, J. Mantz, E. Chan, D. Booher, and L. Figueroa, "Broad-band emission from a multiple asymmetric quantum-well light-emitting diode," *IEEE Photon. Technol. Lett.*, vol. 3, pp. 436–438, 1991.
[67] G. Vermeire, L. Buydens, P. Van Daele, and P. Demeester, "Side-emitting GaAs/AlGaAs SQW single quantum well LED's showing wide spectrum using shadow masked growth," *Electron. Lett.*, vol. 28, pp. 903–905, 1992.

J. J. Coleman, (S'73–M'76–SM'80–F'92) for photograph and biography, see this issue, p. 710.

R. M. Lammert received the B.S. degree in 1993 with highest honors, the M.S. degree in 1995, and the Ph.D. degree in 1997, all in electrical engineering from the University of Illinois, Urbana-Champaign.

He currently is with Ortel Corporation, Alhambra, CA. His research interests are in III-V compound semiconductor quantum-well lasers grown by metalorganic chemical vapor deposition and selective-area epitaxy.

M. L. Osowski received the B.S. degree in engineering physics in 1992 and the M.S. degree in electrical engineering in 1995, from the University of Illinois, Urbana-Champaign, where he is currently working towards the Ph.D. degree in electrical engineering.

His research is concentrated on compound semiconductor epitaxial crystal growth and the development of integratable and integrated semiconductor laser structures for photonic integrated circuit applications.

A. M. Jones received the B.S. degree with honors in 1993 and the M.S. degree in 1995 in electrical engineering, from the University of Illinois, Urbana-Champaign, where he is currently working towards the Ph.D. degree.

Using conventional and selective-area MOCVD, he has focused his research efforts on the growth, modeling, and fabrication of III-V compound semiconductor quantum-well lasers on traditional InP and GaAs binary substrates and on InGaAs ternary substrates.